A Novel Model to Predict the Corrosion of Mechanically Stabilized Earth Structures

Victor Padila, PhD Candidate, Department of Materials Engineering, University of British Columbia

Pouria Ghods, PhD, P.Eng, Department of Materials Engineering, University of British Columbia

Akram Alfantazi, PhD, P.Eng, FCIM, FNACE, FEIC, Department of Materials Engineering, University of British Columbia

Paper prepared for presentation
at the Innovation in Geotechnique for Transportation Session
of the 2013 Conference of the
Transportation Association of Canada
Winnipeg, Manitoba

Abstract:

Early failure of mechanically-stabilized earth (MSE) walls has been often attributed to the corrosion of galvanized steel soil reinforcements on facings. Galvanized steel is one of the most common materials used in the construction industry for its relatively compared to steels with higher corrosion resistance. A numerical model was developed to calculate the corrosion rate of galvanized steel in soil at three different stages of corrosion by considering key soil corrosion parameters such as resistivity, temperature, moisture content, pH, and oxygen availability. This paper focuses on the effect of temperatures relevant to the Canadian climate, and differential soil compaction (related to oxygen access) on the corrosion performance of MSE wall soil reinforcement and facings. Results indicate that the proposed model is suitable to be used for the service-life design and risk assessment of MSE walls and to determine the optimum zinc cover thickness.

1. Introduction

Mechanically-stabilized earth (MSE) walls are typically used to provide support for the backfill of a wide variety of military, and civil engineering projects. The advantages of these structures lie in their cost-effectiveness, rapid construction, and minimization of occupied ground area and high tolerance of differential settlements [1]. MSE walls generally consist of three major structural components (Figure 1): the vertical facing element, the leveling pad, and the reinforced backfill soil [2]. The backfill soil is typically reinforced by steel or geosynthetics mesh which supports the vertical facing element of the system. The properties of the backfill material are selected and controlled prior to construction, but wetting and diffusion of corrosive agents can change the backfill characteristics and can render it corrosive. These corrosive agents can be introduced either by global pollution, marine atmosphere pollutions, floods, de-icing salts, or groundwater pollution [3, 4]. Regardless of the contamination mechanism, the main reason for premature failure in steel-reinforced concrete structures is corrosion of the steel reinforcement [5-7].

MSE walls are typically designed to have a minimum service life of 75 years and have gained widespread acceptance in North America during the past 35 years because of their cost-effectiveness and versatility [8]. However, the durability performance of the reinforcement in soil have raised some controversies such that some researchers believe that the current AASHTO model for the corrosion estimate is unnecessarily conservative [9,10], while on the other hand, the early failure of some MSE walls due to the corrosion of steel have raised concerns about the adequacy of the design requirements [11].

Because of its proven efficiency, coupled with its low cost, galvanized steel is the recommended material for corrosion protection by the CAN/CSA-S6-06 Canadian Highway Bridge Design Code [12], and the American Association of State Highway and Transportation Officials (AASHTO) [8]. Improved performance is provided by the combination of three distinct mechanisms: the barrier action of the zinc layer, the secondary barrier action of the zinc corrosion products, and the cathodic protection of zinc when steel is exposed [13-15]. Unlike Epoxy Coated Reinforces (ECR), even if the coating is subjected to abrasion prior to or during

installation, the overall corrosion resistance of the steel will not be compromised as much as when the ECR is damaged during installation. The corrosion of galvanized steel is a very complex process that involves several electrochemical and physical mechanisms. Studies on the corrosion of galvanized steel revealed that the corrosion behaviour of galvanized steel consisted of three different stages as shown in Figure 2 [13,15]: In Stage 1, the electrochemical behavior of galvanized steel is mainly related to the dissolution of the zinc oxide layer which was formed in the air. In Stage 2, the surface of the zinc layer is covered with thick, white rust and the underlying steel begins to corrode. During this stage, the corrosion rate rapidly decreases, accompanied by a shift in the corrosion potential to noble potential. This indicates that the anodic dissolution of zinc is inhibited in this stage. In Stage 3, the amount of red rust on the coating surface rapidly increases; the galvanized steel shows almost the same corrosion potential as that of carbon steel, even though the zinc coating is still covering a few parts of the rebar. The underlying steel corrosion progresses by dissolution of iron and, therefore, at this stage the zinc coating no longer acts as sacrificial anode.

This research paper presents the development of a novel deterministic model for the corrosion rate determination of galvanized steel in soil. The developed model simulates all three stages of the galvanized steel corrosion process. This paper focuses on the effect of temperatures relevant to the Canadian climate, and differential soil compaction (related to oxygen access) on the corrosion performance of MSE walls and their facings.

2. Modelling Concept

The proposed model simplifies the corrosion of galvanized steel in soil into three different stages briefly explained above.

Each of these stages involves different anodic and cathodic half-cell reactions of both iron and zinc. In the first stage, the corrosion of the galvanized steel is modeled so that the zinc layer is dissolved by anodic reaction and oxygen reduction takes place on the surface of the zinc layer as a cathodic reaction. In the second stage, once the zinc layer is removed by the corrosion process, the underlying steel is exposed to the contaminated soil. As a result, the steel dissolution starts at the corroding site coupled by oxygen reaction in the non-corroding site on the surface of the remaining zinc layer. In the last stage of corrosion, once a sufficiently large amount of the zinc layer is dissolved, the corrosion of underlying steel continues at the corroding site, and the oxygen reduction now occurs on the surface of the underlying steel instead of the zinc layer.

In Stage 1, the anodic reaction takes place on the zinc coating, and thus the zinc dissolves into the pore solution as described in equation 1, and the cathodic reaction is the oxygen reduction as described in equation 2:

$$Zn \rightarrow Zn^{2+} + 2e^{-} \qquad (1)$$

$$O_2 + 2H_2O + 4e^{-} \rightarrow 4(OH^{-}) \qquad (2)$$

The transport of electrons from the anodic region to the cathodic region is attributed to the corrosion current in reinforcement. In this stage, the initial microcell corrosion current density of zinc, $i_{cor,mic}$ (A/m^2), can be easily calculated from exchange current density following the polarization and the mix potential theories [16] as follows:

The anodic reaction takes place through activation polarization as

$$\phi_{a,Zn} = \phi^0_{a,Zn} + \underbrace{\beta_{a,Zn} log(\frac{i_a}{i_{oa,Zn}})}_{Activation} \qquad (3)$$

where $\phi_{a,Zn}$ (V) is the anodic corrosion potential of zinc, $\phi^o{}_{a,Zn}$ (V) is the equilibrium potential of the anodic reaction of zinc, $\beta_{a,Zn}$ is the anodic Tafel slope (V/dec), and $i_{oa,Zn}$ (A/m^2) is the exchange current density of zinc.

The cathodic reaction has both activation and concentration polarization components due to the limiting effect created by oxygen availability around the cathodic sites in the soil as

$$\phi_{c,Ox} = \phi^0_{c,Ox} + \underbrace{\beta_{c,Ox} log(\frac{i_c}{i_{oc,Ox}})}_{Activation} + \underbrace{\frac{2.303RT}{z_c F} log(\frac{i_L}{i_L - i_c})}_{Concentration} \qquad (4)$$

where $\phi_{c,Ox}$ (V) is the cathodic corrosion potential, $\phi^o{}_{c,Ox}$ (V) is the equilibrium potential of the cathodic reaction, $\beta_{c,Ox}$ is the cathodic Tafel slope (V/dec), $i_{oc,Ox}$ (A/m^2) is the exchange current density of the cathodic reaction, i_L (A/m^2) is the limiting current density, R (≈8.314 J/(mole.K)) is the universal gas constant, F (≈96500 C/mole) is the Faraday's constant, T (^{o}K) is temperature, and Z_c is number of electrons that are involved in the cathodic reaction. The limiting current density, i_L (A/m^2), is a measure of oxygen availability around the cathodic sites on the metal surface [17] and in the proposed model, is defined by Eq. 5 as a function of distance to free surface of soil, x (m), oxygen diffusion coefficient, D_{O_2} (m^2/s), and amount of dissolved oxygen on the surface of reinforcement, $C^s_{O_2}$ (mole/m^3) [18]:

$$i_L = z_c F \frac{D_{O_2} C^s_{O_2}}{x} \qquad (5)$$

In this first stage, once the electrochemical equilibrium on the zinc coating surface is reached, the rates of anodic and cathodic reactions, i_a (A/m^2) and i_c (A/m^2) respectively, will be equal to the microcell corrosion current density, $i_{,mic}$. In the microcell corrosion mechanism the distance between the anodic and cathodic sites of reinforcement are very small. Therefore, the effect of soil resistivity (i.e., *IR* drop) can be ignored [19], and the potentials of anode and cathode can be considered the same. As a result, from the solution of two simultaneous equations (i.e., Eq. 3 and

Eq. 4) the microcell corrosion current density, $i_{cor,mic}$, on the surface of zinc in the soil can be derived using equation 6.

$$\phi^0_{c,Ox} - \phi^0_{a,Zn} + \beta_{c,Ox}\log(\frac{i_{cor,mic}}{i_{oc,Ox}}) - \beta_{a,Zn}\log(\frac{i_{cor,mic}}{i_{oa,Zn}}) + \frac{2.303RT}{z_cF}\log(\frac{i_L}{i_{L-}i_{cor,mic}}) = 0 \qquad (6)$$

In the non-corroding site, due to the formation of the zinc oxide, the corrosion mechanism of the anodic microcell reaction is not just a function of the activation polarization equation given in Eq. 3, but it is also important to account for the electrical resistance of the zinc corrosion product as follows:

$$\phi_{a,Zn} = \phi^0_{a,Zn} + \beta_a\, log(\frac{i_a}{i_{oa,Zn}}) + i_a.R_{f,Zn} \qquad (7)$$

where $\phi_{a,Zn}$ (V) is the anodic corrosion potential of zinc in the non-corroding site, $R_{f,Zn}$ ($\Omega.m^2$) is the electrical resistance of the zinc corrosion product, and i_a (A/m^2) is the anodic current density of zinc in the non-corroding site. The polarization curve of the cathodic microcell activity in the non-corroding site still follows the same polarization behaviour as described in equation 4.

At the equilibrium condition the rates of anodic and cathodic reactions, i_a (A/m^2) and i_c (A/m^2) respectively, on the surface of reinforcement are equal to each other and to the microcell corrosion current density, $i_{non\text{-}cor,mic}$. Thus,

$$\phi^0_{c,Ox} - \phi^0_{a,Zn} + \beta_{c,Ox}\log(\frac{i_{non-cor,mic}}{i_{oc,Ox}}) - \beta_{a,Zn}\log(\frac{i_{non-cor,mic}}{i_{oa,Zn}}) + \frac{2.303RT}{z_cF}\log(\frac{i_L}{i_{L-}i_{non-cor,mic}}) - i_{non-cor,mic}.R_{f,Zn} = 0 \qquad (8)$$

The simultaneous solution of Eqs. 6 and 8 provides the microcell corrosion current density in the non-corroding zone ($i_{non\text{-}cor,mic}$) and corroding zone ($i_{cor,mic}$) of the reinforcement. Furthermore, by substituting these values in equations 3 and 7, the microcell corrosion potential in both the non-corroding site ($\phi_{non-cor,mic}$) and the corroding site ($\phi_{cor,mic}$) are determined.

Since the corrosion potential of the corroding site ($\phi_{cor,mic}$) is not the same as that of the non-corroding site ($\phi_{non-cor,mic}$) (i.e., $\phi_{cor,mic} < \phi_{non-cor,mic}$), the macrocell corrosion current is produced to stabilize the imbalanced situation such that

$$\phi_{non-cor,mac} - \phi_{cor,mac} = IR_{soil} \qquad (9)$$

where $\phi_{non\text{-}cor,mac}$ (V) and $\phi_{cor,mac}$ (V) are the macrocell corrosion potentials of the non-corroding site and the corroding site, respectively, R_{soil} (Ω) is the soil resistance, and I (A) is macrocell corrosion current which is equal to $(i_{cor,mac} \times A_{cor})$ or $(i_{non\text{-}cor,mac} \times A_{non\text{-}cor})$ where A_{cor} and $A_{non\text{-}cor}$ are the area of the corroding and non-corroding sites, respectively.

During Stage 2, the zinc cover partially dissolves and the underlying steel is exposed to the soil and also becomes involved in the corrosion reaction based on the following electrochemical reaction:

$$Fe \rightarrow Fe^{2+} + 2e^{-} \qquad (10)$$

In this stage, the anodic reaction of steel takes place through activation polarization as:

$$\phi_{a,Fe} = \phi^{0}_{a,Fe} + \underbrace{\beta_{a,Fe} \log\left(\frac{i_a}{i_{oa,Fe}}\right)}_{Activation} \qquad (11)$$

The cathode polarization equation is the same as the one defined in Equation 4. Since in this stage the distance between the corroding site and non-corroding site of reinforcement is substantial, the microcell corrosion current will be the governing mechanism of corrosion and therefore the role of the soil resistivity becomes important, and the macrocell corrosion will proceed as described in Equation 9. Due to this macrocell corrosion current, the microcell activities in the non-corroding zone and corroding zone are also affected. Macrocell current shifts the anodic current density towards larger values while the cathodic current density of the same segment becomes smaller.

In Stage 3 the zinc coating layer is completely removed from the surface of steel, the effect of zinc in the corrosion process of reinforcement can be discarded, and the steel is involved in the anodic reaction at both the corroding and non-corroding sites. Because of this, at the corroding site, the anodic reaction is mainly governed by iron dissolution (Eq. 10) and at the non-corroding sites the oxygen reduction controls the cathodic reactions (Eq. 2). In this stage, the corrosion mechanism of galvanized steel would be very similar to the bare steel metal and by solving Eqs. 4, 9 & 11 the corrosion rate of reinforcement would be determined [20].

In the non-corroding site, the polarization reaction follows the modified anodic polarization equation as

$$\phi_{a,Fe} = \phi^0_{a,Fe} + \beta_{a,Fe} log(\frac{i_a}{i_{oa,Fe}}) + i_a.R_{f,Fe} \qquad (12)$$

The polarization curve of the cathodic microcell activity still follows the same equation as the cathodic polarization Equation 4. At the equilibrium condition, similar to the procedure described above, the microcell corrosion current density, $i_{non\text{-}cor,mic}$, is identical to the rates of anodic (i_a (A/m^2)) and cathodic reactions (i_c (A/m^2)). Thus,

$$\phi^0_{c,Ox} - \phi^0_{a,Fe} + \beta_{c,Ox} \log(\frac{i_{non-cor,mic}}{i_{oc,Ox}}) - \beta_{a,Fe} \log(\frac{i_{non-cor,mic}}{i_{oa,Fe}}) + \frac{2.303RT}{z_c F} \log(\frac{i_L}{i_L - i_{non-cor,mic}}) - i_{non-cor,mic}.R_{f,Fe} = 0 \quad (13)$$

by solving Eqs. 6 and 13, the microcell corrosion current density in the non-corroding site ($i_{non\text{-}cor,mic}$) and corroding site ($i_{cor,mic}$), as well as the microcell corrosion potential of the non-corroding site ($\phi_{non-cor,mic}$) and corroding site ($\phi_{cor,mic}$) are determined. Since the corrosion potential of the corroding and non-corroding site is different, the macrocell corrosion current is produced to balance the situation (Eq. 9).

3. Numeral Solution

The one-dimensional simplification explained above is useful to theoretically describe microcell and macrocell corrosion of galvanized steel reinforcement in soil; however, the solution of the problem needs to be conducted in the two-dimensional domain. As a result, a non-linear finite element approach was used to solve the Laplacian differential equation of potential distribution in the conductive media of soil as described by

$$\nabla.(\frac{1}{\rho_{soil}}.\nabla\phi) = 0 \qquad (14)$$

where ϕ (V) is the electrical potential and ρ_{soil} (Ω.m) is the soil resistivity.

As shown in Figure 3, a rectangular domain resembling the 2-D geometrical conditions of reinforcement in the soil was considered in this study for numerical analysis. The nodal potential of the domain was determined by finite element solution of Eq. 14 and accordingly the potential gradient at each element of the domain (defined by index *i*) was calculated in both the corroding and non-corroding sites (i.e., i_{cor} and $i_{non\text{-}cor}$) using Ohm's law, and calculated from equations 15 and 16:

$$i_{cor}^{i} = -\frac{1}{\rho_{soil}}\frac{\partial\phi^{i}}{\partial n} \qquad (15)$$

$$i_{non-cor}^{i} = -\frac{1}{\rho_{soil}}\frac{\partial\phi^{i}}{\partial n} \qquad (16)$$

where ρ_{soil} (Ω.m) is the soil resistivity, and n is the direction normal to the equipotential lines. Since the mechanism of galvanized steel corrosion in the soil is the combination of macrocell and microcell corrosion [21], in the numerical simulation of the corrosion process the effect of macrocell corrosion activity needs to be considered on the microcell corrosion activity at each node on the surface of reinforcement. In order to take this effect into the consideration, the electrical neutrality equation was also satisfied along with equations 14 to 16 in the both corroding and non-corroding zones of the reinforcement. As a result, in all three corrosion stages, the summation of any imbalanced amount of anodic and cathodic current density at each node was set equal to each other as:

$$\sum_{i=1}^{n}(i_{c,cor}^{i} - i_{a,cor}^{i}) = \sum_{i=1}^{n}(i_{c,non-cor}^{i} - i_{a,non-cor}^{i}) \qquad (17)$$

The analysis was carried out in a 2-D rectangular domain that was 300 mm long and 100 mm wide (Fig. 3); the domain was discretized by triangle finite elements. The element size was optimized to achieve a balance between accuracy and numerical efficiency. The values of the constant parameters used in this study (e.g. exchange current densities, Tafel slopes, etc.) are presented in Table 1. These constants were selected to represent typical values reported in the literature for each stage of galvanized steel corrosion in soil [22-28].

4. Results and Discussion

A user friendly program was developed in MATLAB software to simulate the numerical model described earlier in this paper. A series of analyses were carried with the software to calculate the corrosion rate of galvanized steel reinforcement at the three stages for several cases. Those cases were chosen so as to study the influence of the parameters that significantly affect the corrosion rate of galvanized steel in the soil such as the temperature and oxygen concentration. The details of each study will be discussed separately.

Effect of Temperature:

A previous study [29] showed that decreasing temperature has a considerable effect on the corrosion current of galvanized steel in corrosive solutions. Nonetheless, the corrosion rate observed at sub-zero temperatures is still higher than the rate acceptable for galvanized steel reinforced structures. The increased corrosion rate was attributed to the presence of corrosive agents, namely NaCl and Na_2SO_4, and confirmed that early structural failure of steel reinforcement can still be a concern in cold regions.

According to the AASHTO specification [9,30], the lower and upper values of the chosen

resistivity respectively resemble an aggressive and non-aggressive environment condition for the soil around the reinforcement. A high value for the limiting current density (i.e., i_L = 60 μA/cm^2) was selected to simulate the condition where the concentration of oxygen around the reinforcement is relatively high and the rate of corrosion process is not controlled by the oxygen diffusion. An aggressive environment is defined by the AASHTO LFRD Bridge Design Specifications as conditions where either chloride concentration is greater than 100 ppm per weight (0.01 %wt), sulphates concentration is higher than 200 ppm per weight (0.02 %wt), the soil resistivity is lower than 3000 ohm.cm, the pH is out of the range of 5 to 10, or the organic or moisture contents are larger than 1 weight percent (wt%) [9,30]. The effect of temperature was investigated by varying temperature from -5 ºC to 35 ºC.

Figure 4 shows the effect of temperature at three different soil resistivity values: 2500 Ω·cm, 7500 Ω·cm, and 15000 Ω·cm to simulate from highly corrosive conditions, to non-corrosive conditions. Other important key parameters were fixed to isolate the effect of temperature; the pH was set at 7, moisture content at 1 wt%, and the limiting current density at 60 μA/cm^2. Fig. 4a shows the effect of temperature on Stage 1 of the corrosion of galvanized steel. It is possible to see that in highly aggressive conditions, resistivity 2500 Ω·cm, the calculated corrosion rate is higher at any temperature than the limit established by AASHTO, shown in the figure with the grey line (15μm/year, 4 μm/year, and 12 μm/year for Stage 1, Stage 2 and Stage 3, respectively). It is also possible to notice that, when the soil resistivity is 7500 Ω·cm, the corrosion rate might become a concern at temperatures higher than 10 ºC. And finally, in non-corrosive conditions, when the soil resistivity is high enough to hinder the flow of electrons 15000 Ω·cm, the corrosion rate stays below the limit set by AASHTO at any temperature.

Fig. 4b shows the effect of temperature on Stage 2 of the corrosion of galvanized steel. Similar to the behaviour observed in Stage 1, in highly aggressive conditions, the calculated corrosion rate of is higher at any temperature than the limit established by AASHTO. This same response to temperature is observed when the soil resistivity is 7500 Ω·cm, and in non-corrosive conditions, soil resistivity set at 15000 Ω·cm, the corrosion rate becomes higher than the limit established by AASHTO at temperatures higher than 10 ºC. This indicated that the second stage

of the corrosion of galvanized steel is perhaps very sensitive to both soil resistivity and temperature, and almost in any condition the corrosion rate could become a problem.

Figure 4c shows the effect of temperature on Stage 3 of the corrosion of galvanized steel; again a very similar response is observed. In highly aggressive conditions, the calculated corrosion rate is higher at any temperature than the limit established by AASHTO. When the soil resistivity is 7500 Ω·cm, the corrosion rate surpasses the allowed limit in temperatures above the freezing point of water, and in non-corrosive conditions, when the soil resistivity set at 15,000 Ω·cm, the corrosion rate becomes higher than the limit established by AASHTO at temperatures higher than 25 ºC; indicating that the corrosion rate during the third stage of the corrosion could be a problem in mildly aggressive conditions, or in warm periods of the year.

Effect of Oxygen:

When either the amount of oxygen or the corrosive medium conductivity increases, it is expected that the corrosion process will be enhanced. A number of different factors can promote the conditions to have a variable oxygen access on a structure: partial immersion of the structure in an aquatic/marine environment; partial coverage of the reinforcement by concrete, or simply a gradient in the soil compaction [31]. Previous work revealed that an increased concentration of oxygen appears to have a greater effect on the corrosion rate than the presence of corrosive agents in the environment [31]. Furthermore, differential oxygen access is expected to promote corrosion macrocells, with the cathode on the site with the higher oxygen content [32] and with possible corrosion enhancement near the high stress regions. In this work, the effect of oxygen concentration on the corrosion rate of galvanized steel is assessed through the limiting current density (i_L). The general assumption is that greater oxygen availability will result in an increased limiting current density value, ultimately increasing the corrosion rate. In this paper, the corrosion rate of galvanized steel at each stage of corrosion was calculated for various values of the limiting current densities ranging from 20 to 70 $\mu A/cm^2$.

Figure 5 show the effect of limiting current density (i.e., oxygen concentration) at three different soil resistivity values: 2500 Ω·cm, 7500 Ω·cm, and 15000 Ω·cm. The other key

parameters were fixed to isolate the effect of oxygen concentration; the pH was set at 7, moisture content at 1 wt%, and temperature at 25 ºC. When comparing Fig. 5a, Fig 5b and Fig. 5c one can conclude that, according to the proposed model, the first stage of corrosion is more sensitive to oxygen concentration variation that the other two stages. However, in all different stages the corrosion rate increases with increasing limiting current density. It is also possible to notice in Fig. 5a that the effect of oxygen concentration seems to be more pronounced in highly corrosive environments (e.g low soil resistivity). The differences in corrosion rate, at all different stages, when the soil resistivity is set at 7,500 Ω·cm, and 15,000 Ω·cm seems to be not too significant, and generally the corrosion rate reaches a plateau with limiting current density values greater than 30 $\mu A/cm^2$. Fig 5c shows that the increasing the limiting current density values (i.e., increasing oxygen concentration) seems to have little effect on the third stage of corrosion of galvanized steel. However, according to the results shed by the proposed model, it seems that corrosion rates always exceed the limits set by the AASHTO model.

5. Conclusions

In this study, the effect of temperature and limiting current density (i.e., oxygen concentration) on the three stages of galvanized steel corrosion were numerically investigated. The corrosion rate of galvanized steel at each stage of the corrosion process increases with increasing temperature. Decreasing the access of oxygen to the structures will lead to a decrease in the rate of corrosion. And finally, the presented model is a practical tool for engineers since it is able to estimate corrosion damage evolution with good approximation, while the variables can be easily adjusted to consider any specific soil environment and climatic conditions. Therefore, the model can be practically used to determine optimum zinc cover thickness and to estimate the remaining service life of the existing MSE walls.

Acknowledgments

The authors would like to express their gratitude to the British Columbia Ministry of Transportation for the financial support provided for this work, in particular to Kevin Baskin for the valuable insights and support provided. The second author would also like to thank the

NSERC for the financial support provided through the Postdoctoral Research Fellowship program.

References

[1] Ng, C., Chew, S., Karunaratne, G., Tan, S., and Loh, S. Flexible and Rigid Faced MSE Walls Subject to Blasting, Advances in Transportation and Geoenvironmental Systems Using Geosynthetics. (2000) 322-336.

[2] C Yohchia. Practical analysis and design of mechanically-stabilized earth walls—I. Design philosophies and procedures, Eng.Struct. 22 (2000) 793-808.

[3] E Bourgeois, A Corfdir, T Chau. Analysis of long-term deformations of MSE walls based on various corrosion scenarios, Soils and Foundations. 53 (2013) 259-271.

[4] V Padilla, P Ghods, A Alfantazi. Effect of de-icing salts on the corrosion performance of galvanized steel in sulphate contaminated soil, Constr.Build.Mater. 40 (2013) 908-918.

[5] AP Yadav, H Katayama, K Noda, H Masuda, A Nishikata, T Tsuru. Effect of Fe-Zn alloy layer on the corrosion resistance of galvanized steel in chloride containing environments, Corros.Sci. 49 (2007) 3716-3731.

[6] W Aperador, R Mejia de Gutierrez, DM Bastidas. Steel corrosion behaviour in carbonated alkali-activated slag concrete, Corros.Sci. 51 (2009) 2027-2033.

[7] DM Bastidas, A Fernandez-Jimenez, A Palomo, JA Gonzalez. A study on the passive state stability of steel embedded in activated fly ash mortars, Corros.Sci. 50 (2008) 1058-1065.

[8] V. Elias. Corrosion/Degradation of Soil Reinforcements for Mechanically Stabilized Earth Walls and Reinforced Soil Slopes, FHWA-NHI-00-044 (2000) 1-94.

[9] R.A. Gladstone, P.L. Anderson, K.L. Fishman, J.L. Withiam. Durability of Galvanized Soil Reinforcement: More Than 30 Years of Experience with Mechanically Stabilized Earth, Transportation Research Record: Journal of the Transportation Research Board. 1975 (2006) 49-59.

[10] K Fishman L, JL Withiam. LRFD Metal Loss and Service-Life Strength Reduction Factors for Metal-Reinforced Systems, NCHRP REPORT 675. Project 24-28 (2011).

[11] T. A. Armour, J. Bickford, T Pfister. Repair of Failing MSE Railroad Bridge Abutment, ASCE Conf. Proc. Geotechnical Special Publications GSP 136 (2004) 1-15.

[12] Canadian Standards Association, CAN/CSA-S6-06 Canadian Highway Bride Design Code, Published in November 2006, approved by Standards Council of Canada, .

[13] GA El-Mahdy, A Nishikata, T Tsuru. Electrochemical corrosion monitoring of galvanized steel under cyclic wet–dry conditions, Corros.Sci. 42 (2000) 183-194.

[14] A Macias, C Andrade. The behaviour of galvanized steel in chloride-containing alkaline solutions-I. The influence of the cation, Corros.Sci. 30 (1990) 393-407.

[15] AP Yadav, A Nishikata, T Tsuru. Electrochemical impedance study on galvanized steel corrosion under cyclic wet–dry conditions—influence of time of wetness, Corros.Sci. 46 (2004) 169-181.

[16] DA Jones. Principles and Prevention of Corrosion, second ed. Prentice Hall. (1995).

[17] H Bohni. Corrosion in Reinforced Concrete Structures, CRC Press, New York. (2005).

[18] M Pour-Ghaz, OB Isgor, P Ghods. The Effect of Temperature on the Corrosion of Steel in Concrete. Part 2: Model Verification and Parametric Study, Corros.Sci. 51 (2009) 426-433.

[19] J Gulikers. Theoretical considerations on the supposed linear relationship between concrete resistivity and corrosion rate of steel reinforcement, Mater. Corros. 56 (2005) 393-403.

[20] Pour-Ghaz. M, Burkan Isgor, O, Ghods, P. The effect of temperature on the corrosion of steel in concrete. Part 1: Simulated polarization resistance tests and model development, Corros.Sci. 51 (2009) 415-425.

[21] RW Revie, HH Uhlig. Corrosion and Corrosion Control, fourth ed. John Wiley & Sons. (2008).

[22] RD Armstrong, MF Bell. The Electrochemical Behaviour of Zinc in Alkaline Solution, Electrochemistry in: H.R. Thirsk, Editor, The Chemical Society. (1974) 1-17.

[23] S Stankovic, B Grgur, N Krstajic, M Vojnovic. Kinetics of the zinc anodic dissolution reaction in near neutral EDTA solutions, J. Serb. Chem. Soc. 68 (2003) 207–218.

[24] XG Zhang. Corrosion and Electrochemistry of Zinc, Plenum Press, New York. (1996).

[25] SJ Chung, YK Kim. Hydrodynamic and Atmospheric Effects on Corrosion of Zinc in Borate Buffer Solution, J. Korean Chem. Soc. 55 (2011) 575-580.

[26] M Sakairi, Y Uchida, T Kikuchi, H Takahashi. Influence of Zinc Ions on Initial Stage of Localized Corrosion of Zn and Zn–Al Alloy Coated Steels with Photon Rupture Method, ISIJ International. 48 (2008) 988–993.

[27] Z Pilbáth, L Sziráki. The electrochemical reduction of oxygen on zinc corrosion films in alkaline solutions, Electrochim.Acta. 53 (2008) 3218-3230.

[28] MC Li, M Royer, D Stien, A Lecante, C Roos. Inhibitive effect of sodium eperuate on zinc corrosion in alkaline solutions, Corros.Sci. 50 (2008) 1975-1981.

[29] V.E. Padilla Perez, A. Alfantazi. Corrosion Performance of Galvanized Steel in Na2SO4 and NaCl solutions at Subfreezing Temperatures Corrosion. (2012).

[30] M Maslehuddin, MM Al-Zahrani, M Ibrahim, MH Al-Mehthel, SH Al-Idi. Effect of chloride concentration in soil on reinforcement corrosion, Constr.Build.Mater. 21 (2007) 1825-1832.

[31] V.E. Padilla Perez, A. Alfantazi, Effects of Oxygen and Sulfate Concentrations on the Corrosion Behavior of Zinc in NaCl Solutions, Corrosion. 68 (2012) 035005-1-035005-11.

[32] A Sagüés, R Scott1, J Rossi, J Peña, R Powers. Corrosion of Galvanized Strips in Florida Reinforced Earth Walls, J. Mater. Civ. Eng. 12 (2000) 220-227.

Table 1: The constant parameters in the developed model

Parameter	Value
Cathodic exchange current density of oxygen ($i_{oc,Ox}$)	0.00001 A/m^2
Anodic exchange current density of iron ($i_{oa,Fe}$)	0.0003 A/m^2
Anodic exchange current density of zinc ($i_{oa,Zn}$)	0.001 A/m^2
Cathodic standard potential of oxygen ($\phi^o_{c,Ox}$)	0.16 V
Anodic standard potential of iron ($\phi^o_{a,Fe}$)	-0.78 V
Anodic standard potential of zinc ($\phi^o_{a,Zn}$)	-1.007 V
Cathodic Tafel slope of oxygen ($\beta_{c,Ox}$)	-0.180 V/dec
Anodic Tafel slope of iron ($\beta_{a,Fe}$)	0.090 V/dec
Anodic Tafel slope of zinc ($\beta_{a,Zn}$)	0.120 V/dec
Ratio of anode area to cathode area	0.1

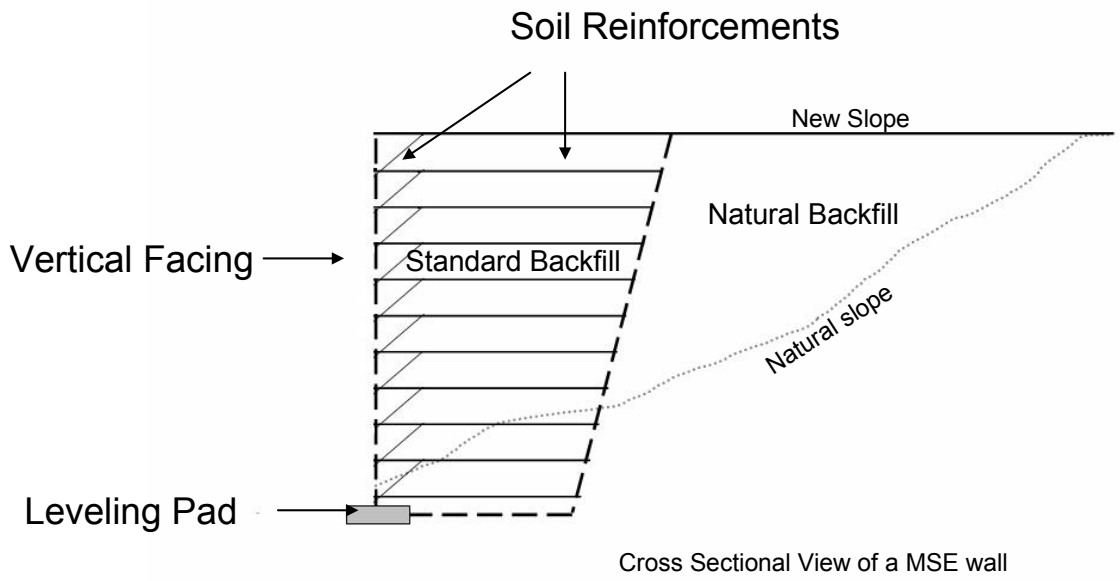

Figure 1- Schematic of a cross sectional view of a typical mechanically stabilized earth wall

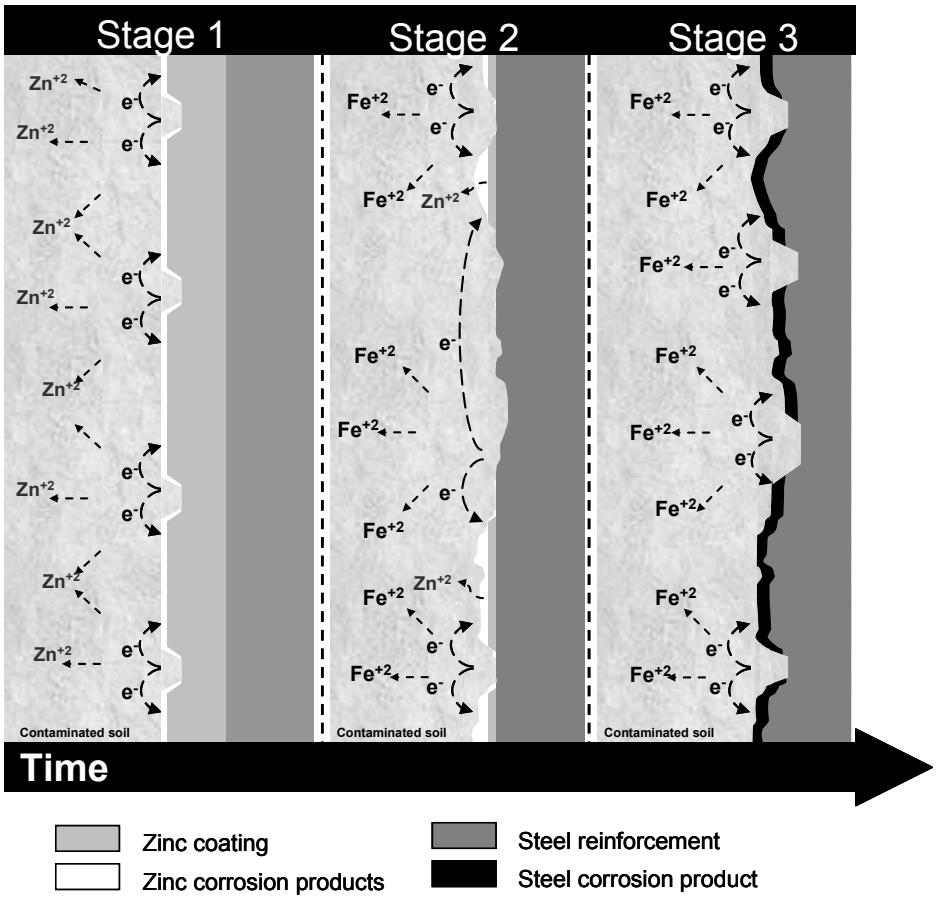

Figure 2- Schematic presentation of the three stages of galvanized steel corrosion

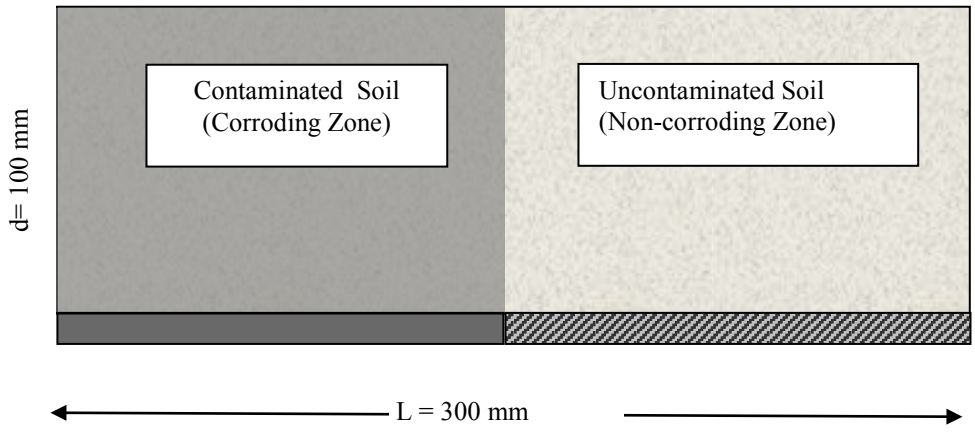

Figure 3- The schematic illustration of microcell and macrocell corrosion of galvanized steel in soil

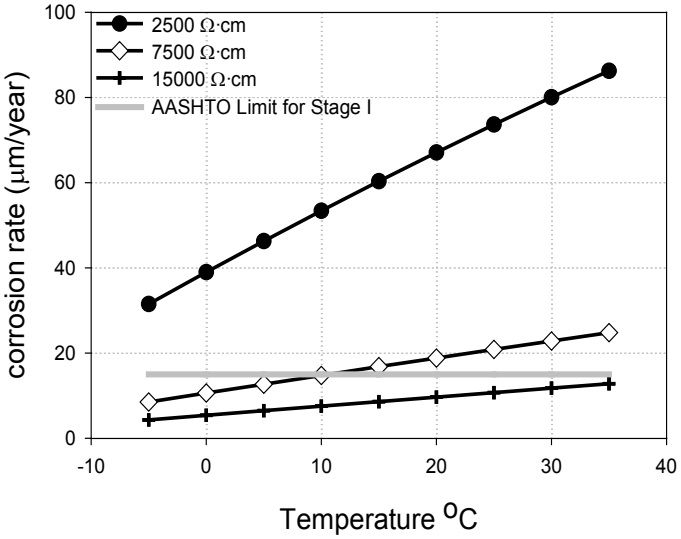

a) Stage 1

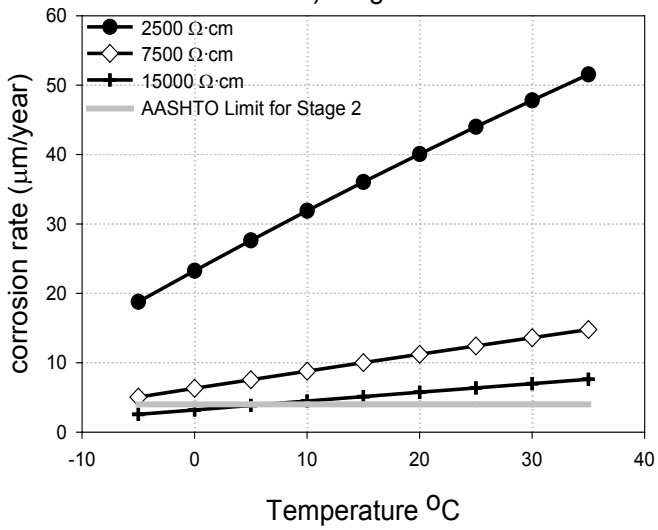

b) Stage 2

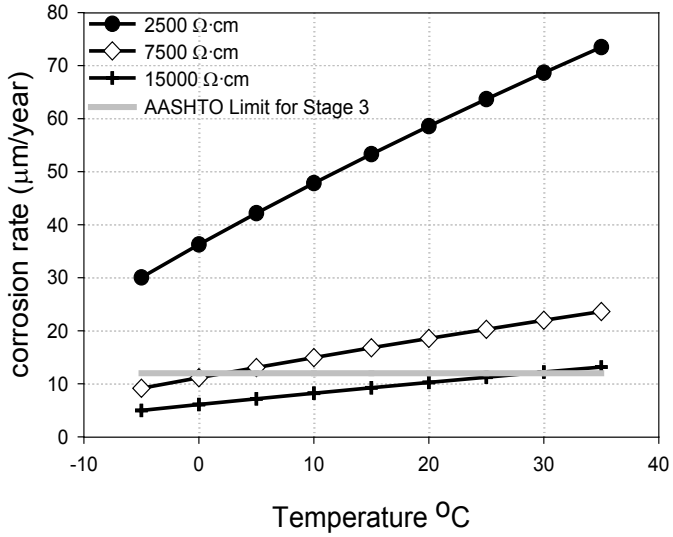

c) Stage 3

Figure 4- The effect of temperature on the three stages of corrosion rate of galvanized steel

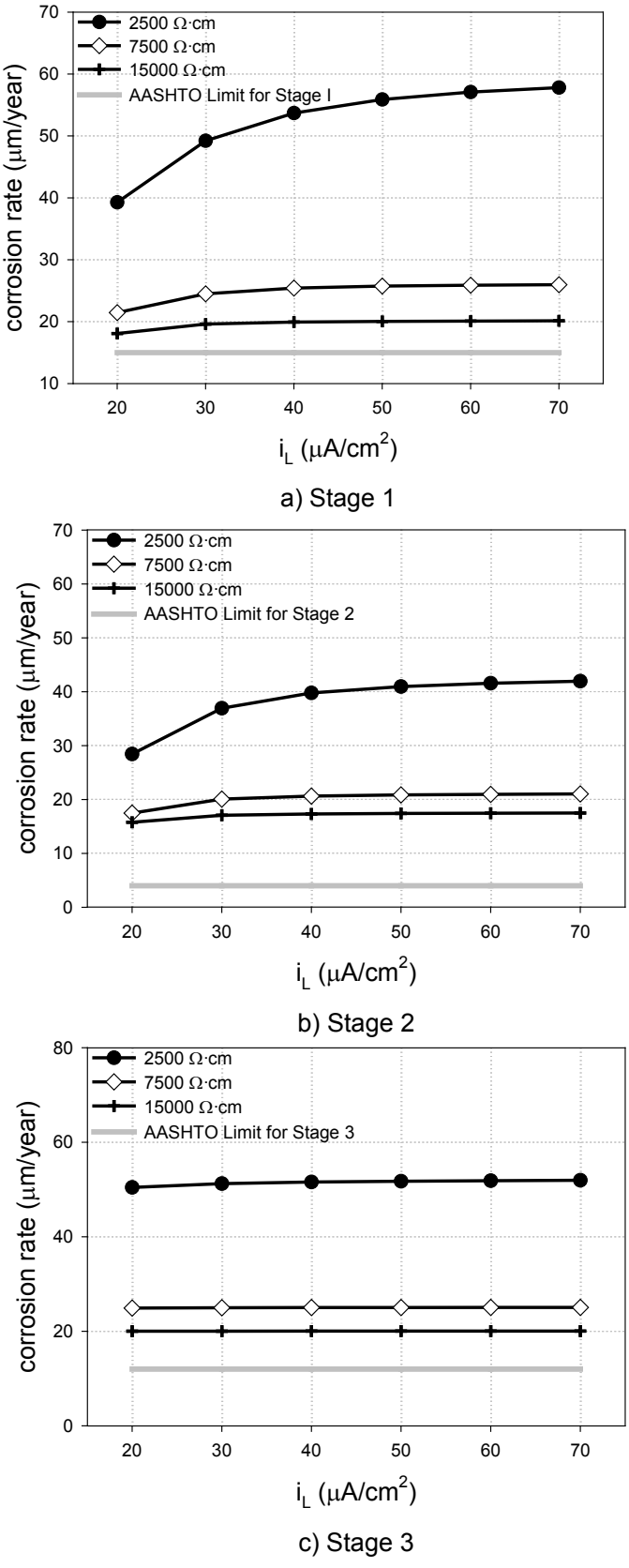

Figure 5- The effect of limiting current density (i.e., oxygen concentration) on the three stages of corrosion rate of galvanized steel